4ICEGE
Thessaloniki-GREECE 2007

4th International Conference on
Earthquake Geotechnical Engineering
June 25-28, 2007
Paper No. 1257

MODELLING OF LIQUEFACTION AROUND TUNNELS

Mark STRINGER [1], Gopal MADABHUSHI[2]

ABSTRACT

This paper investigates the failure mechanisms surrounding the uplifting of pipes in liquefied soil. Shaking table tests under 1g conditions were carried out on a small-scale model of a tunnel buried just below the sand surface. A camera capable of taking hi-speed photo bursts was used to obtain images of the model cross-section throughout the earthquakes. GeoPIV software, an implementation of the Particle Image Velocimetry (PIV) technique, was used to obtain displacement fields in the soil as the tunnel uplifted.

The cumulative displacement field showed soil around the tunnel flowing into the region directly beneath the tunnel, but that the vertical motion of the tunnel during each half cycle of excitation could be broken into three phases. In regions where the magnitude of accelerations decreased, very little displacement occurred in the soil. As accelerations increased close to the maximum magnitude, uplift occurred as soil moved around the tunnel lifting it upwards. The overall vertical displacement was reduced as accelerations reached their maximum in each half cycle. In this period the soil next to tunnel formed a wedge that caused the tunnel to suffer vertical displacement

Keywords: Tunnels, Liquefaction, Failure Mechanism

INTRODUCTION

Where the possibility of soil liquefaction exists, concerns arise about the resistance of buoyant underground structures, such as storage tanks, pipes and tunnels. Case histories where pipes and storage tanks have floated are numerous; Seed and Idriss (1967) report a storage tank experiencing 10ft of floatation during the 1964 Niigata earthquake, while Youd and Hoose (1976) note that during the 1906 San Francisco earthquake, pipeline floatation led to the severing of several major lifelines. Today, concerns exist over the floatation resistance of some tunnels in liquefiable deposits. One particular example is San Francisco's Bay Area Rapid Transport (BART) network. Arango et al. examined the Transbay section of the BART, finding that should an earthquake of magnitude 6.5 or greater strike the area, there would be a 97% chance of liquefaction in the surrounding deposits.

The potential for large loss of life and social & economic disruption caused by a tunnel experiencing floatation makes the study of tunnel floatation essential. Some knowledge exists about the response of pipelines to liquefaction, and possible means of remediation. However, very little is known about the actual soil movements as a tunnel experiences floatation. In 2005, two test series were carried out by Teymur & Madabhushi (2005) and by Cox (2005) with the aim of capturing soil displacements around tunnels and pipes in liquefied soils using the PIV technique presented later in this paper. Both tests used a hollow aluminium pipe section, buried in Fraction E sand. Floatation was observed for tests where the tunnel was buried just beneath the surface, and suctions were observed beneath the tunnel as it uplifted. However, in both cases the image analysis was compromised by sand moving between the tunnel and the viewing window, representing a departure from the plane strain conditions being modeled, and making it impossible to accurately follow the tunnel's movement using

[1] Mark Stringer, Department of Engineering, University of Cambridge, UK, Email: mes38@cantab.net
[2] Dr. Madabhushi, Department of Engineering, University of Cambridge, UK.

photogrammetry. The results were further affected by the thin layer of pore fluid above the soil surface. When earthquakes were fired, the resulting waves of fluid visibly affected the soil just beneath the soil's surface.

With this in mind, this test was designed to eliminate the problems mentioned above and produce high quality data which could be used to obtain the failure mechanism associated with the uplifting of tunnels in liquefied soils. The tests are designed to be carried out under 1g conditions, so concerns exist about the inability to obtain similitude of stresses in the model. However, further tests are scheduled at the Schofield center, which will carry out similar tests on the beam centrifuge. It is hoped the results will validate the mechanisms presented here, and the use of a 1g shaking table for dynamic tests.

EXPERIMENTAL SET UP & TECHNIQUES

Shaking table

Earthquakes were simulated by using a 1g shaking table which applied a sinusoidal displacement, and therefore acceleration, of constant frequency. The shaking table delivers the horizontal excitation by means of a crank. Initially, energy is stored in the system by means of a flywheel, which continues to be accelerated after the earthquake has started so that the desired motion is maintained for the period of excitation. The crank's offset is adjustable so that horizontal amplitudes can be varied in the range 0 – 11mm. The speed of the fly wheel is also adjustable so that the frequency of shaking can be varied between 0 – 4.8Hz. The shaking table is therefore able to supply earthquakes with peak accelerations up to 1g.

Typically, real earthquakes consist of a single strong cycle, followed by many more weaker cycles. The shaking table is unable to replicate these events, since offset can only be changed when the table is stationary. However, the table is adequate for achieving and maintaining a state of liquefaction in saturated soil.

Container

The container used to house the models in all tests had internal dimensions $400 \times 200 \times 500$mm. The front of the box was constructed from Perspex to allow soil movements to be observed. On the inner face of the Perspex, a grid of control markers was created. The control markers consist of a black dot with a circular white background, created from tipex. The control markers were required for the image analysis, which is covered later.

A sheet of sticky back plastic was placed on the inside of the viewing window, covering the control markers. The sticky-back plastic had two functions. The first was to protect the control markers. The second was to help reduce the problem of sand moving in front of the tunnel; The sticky-back plastic helped to smooth out the roughness on the viewing window caused by the control markers.

Sand

Hostun S28 sand was used in the model. The sand's particle size distribution showed no appreciable amount of fines and that the soil was quite poorly graded, making it susceptible to liquefaction. The specific gravity of the sand was 2.65, with a nominal grain size, D_{50} = 0.35mm. Undyed sand was poured into the container using a hopper. The dyed sand, required for image analysis was placed by hand pluviation. A relative density of 0.36 was achieved in the model.

Tunnel

The tunnel was modelled by an aluminium pipe section, with outer diameter 50mm and wall thickness 3.18mm, representing a tunnel of diameter 5m, giving a length scaling factor of 100. The problem was modelled as plane strain, so ideally the interfaces between sides and tunnel would be frictionless.

To aid this, a sheet of glass was attached to the back wall and PTFE end caps were attached to the tunnel at both ends. The combined aluminium pipe and PTFE end caps had a specific gravity G_s = 0.76. When the tunnel was placed in the model, a thin layer of Vaseline was applied to both ends, which helped prevent sand moving in front of the tunnel during the test.

Pore Fluid

Iai et al.(1989) proposed a set of scaling laws for use on 1-g shaking tables. However, dimensional analysis was carried out for this experiment to confirm the results. The group which represented the movement of fluid through the model, which was considered to be the most important, confirmed Iai's scale factor of $n^{1/2}$ for viscosity. The model was therefore saturated with a solution of methyl cellulose with viscosity 10Cst. The solution was prepared using the relationship found empirically by Stewart et al (1998)

A gravel drain, constructed in the back-right corner of the model container allowed the level of the pore fluid to be lowered to the surface level prior to shaking so that the soil disturbances observed in previous tests due to surface waves (Cox, 2005) would not occur.

Instrumentation

Instrumentation inside the model consisted of miniature PPTs made by Druck Ltd. and piezo-electric accelerometers constructed by D.J. Birchall Ltd. A draw-wire potentiometer was used to measure the vertical displacement of the tunnel. An LVDT was used to measure the input excitation, with an additional accelerometer being mounted on the table to verify the input signal.

Image Acquisition and Analysis

Images from the test were obtained using a Photosonics Phantom 5 camera. The camera model has been used previously in applications requiring high resolution images captured at small time intervals, such as crash testing. The camera was used previously by Cox(2005) and Teymur et al. (2005) to acquire images in their experiments.

The camera is capable of capturing greyscale images of resolution 1024x1024 at up to 1000Hz. The camera has an internal memory of 1Gb, on which images are initially stored, so the frequency of image acquisition must be altered to suit the length of experiment being undertaken.

During the experiments undertaken, the camera was set to acquire photos at 100Hz. It was felt that this would ensure enough frames were captured to obtain accurate displacement fields, while still allowing an earthquake of reasonable length to be fired.

Analysis of images was carried out using the geoPIV suite of software, developed by White and Take (2002). The software runs entirely within Matlab, and uses the Particle Image Velocimetry technique to track the position of soil patches through an image sequence.

GeoPIV obtains the displacement fields by tracking the position of patches through pairs of images and comparing relative positions; Fig. 1 shows the principles of PIV. In the first image, the position of the patch is known, and geoPIV works out the patch's 'texture' by examining how the brightness in the image varies spatially through the patch. In the second image, the new position of the patch is located. GeoPIV examines the texture of patches in the second image, first centered at the original position of the patch, and then with the patch centered on individual pixels within a user-defined search zone. Once all possible positions within the search zone have been checked, geoPIV assumes that the patch has moved to the position which gives the best correlation with the first image in the pair. To obtain sub-pixel precision, geoPIV then performs bi-cubic interpolation between the 'best pixel' and its neighbours. This process is repeated for each patch in the image and each image in the sequence. This generates the position of each patch throughout the sequence, allowing displacement fields to be created in image space (pixel co-ordinates).

Control markers, mentioned earlier, consist of a small black dot surrounded by a white background. The real space positions of the control markers are known, and by tracking the control markers through the image sequence in a similar manner to the soil patches, the software is able to apply a further routine to the results which removes the effects of lens imperfections, non-normality of the viewing plane to the camera, and the rigid body motion which exists due to the camera not being mounted on the table during the experiment. The known positions of the markers allows the corrected patch positions to be converted into real space co-ordinates, and hence the true displacement field is created. Further information relating to geoPIV can be found in papers by White and Take (2002) and White et al. (2003)

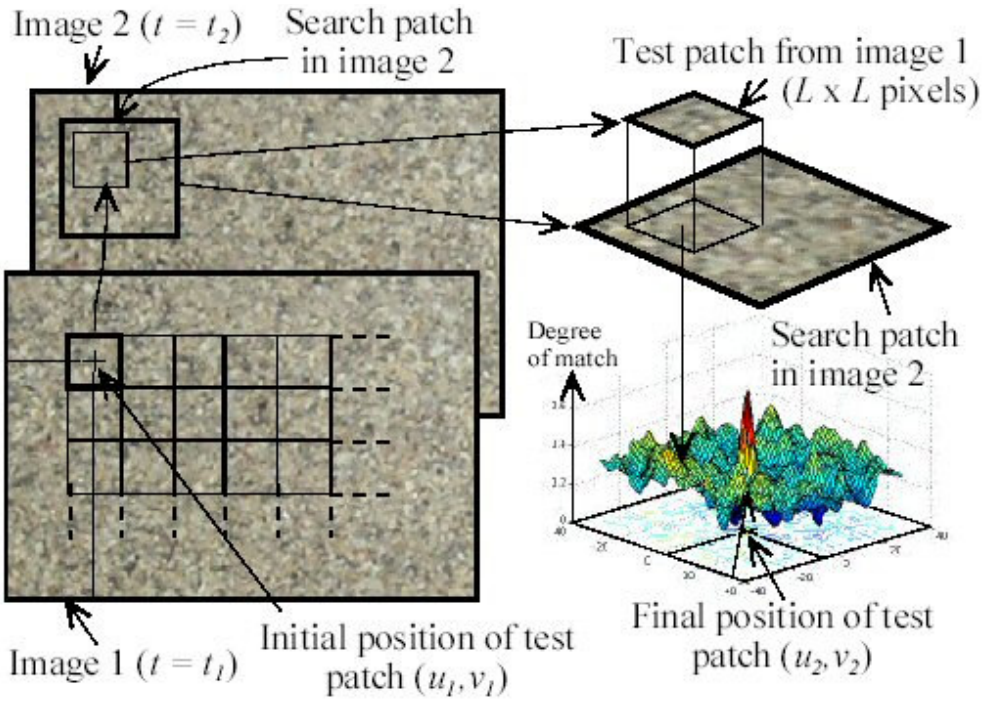

Figure 1. Principles of geoPIV (after White et al, 2003)

FLOTATION OF TUNNELS

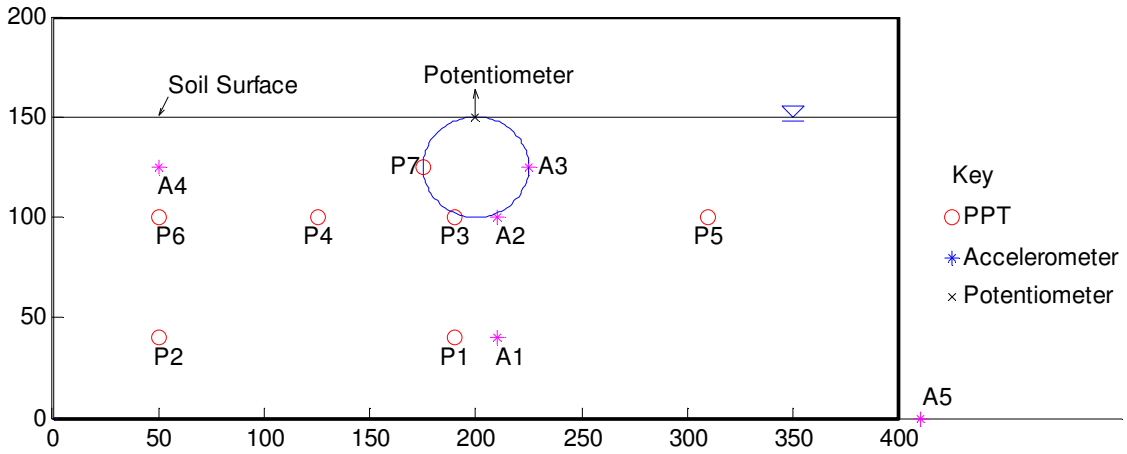

Figure 2. Instrumentation Layout

The tunnel was placed such that the crown of the tunnel was at the soil's surface. A schematic of the model layout is shown in Fig. 2. A total of 3 earthquakes were fired on the model, with maximum accelerations 0.65g, 0.71g and 1.02g.

The tunnel was observed to experience floatation during all three earthquakes, rising 4.21mm, 3.90mm and 1.62mm in the first, second and third earthquakes respectively. The total floatation was 9.73mm, with pictures of the model before and after testing shown in Fig. 3(a) and (b).

During excavation of the model, it was found that with the exception of P7, all instruments retained their original positions. However, P7 was found to have displaced downwards 6mm and laterally towards the tunnel by 12mm.

The results which are discussed in following sections refer to the first earthquake fired, where the largest deformations occurred and the model was in its most undisturbed state.

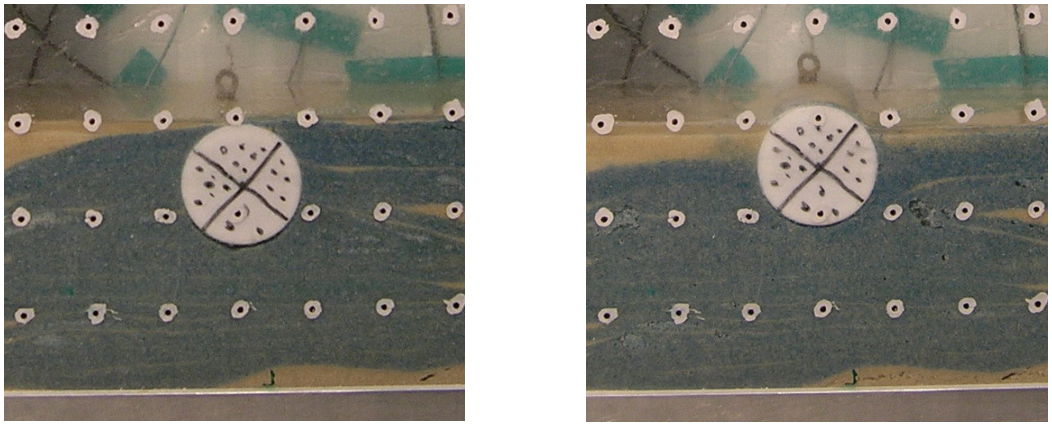

Figure 3.(a) Model before test & (b) Model after testing

Pore Pressures

Fig. 4 shows the pore pressure readings from the test. The small size of the model and the 1g conditions meant that very low positive pore pressures were required for liquefaction. This resulted in the normal build up of excess pore pressures, normally associated with this type of experiment, not being observed. In the frequency domain, the traces show strong components at double the excitation frequency, caused by the soil changing from contractive to dilative behaviour, as it crosses the characteristic state line proposed by Luong and Sidaner, 1981. The component at double frequency became stronger in the later earthquakes, where the maximum accelerations were higher.

PPTs 2 and 6 both show peak values of pore pressure far in excess of those required to reach liquefaction. These two instruments were located close to the side walls of the box. As the soil is being decelerated, it continues to try to displace laterally. However, since the sides of the box are stiff, this will result in a pressure wave being set up near the walls, giving rise to the higher than expected pressures. The idea that the extra excess pore pressure observed during the earthquake comes from pressure waves being set up near the boundaries is supported by the fact that once shaking has ended, the pore pressures immediately show a value which the soil would require for liquefaction, dissipating slowly as expected.

PPTs 3 and 7 show pore pressures being kept very low during the earthquake, before jumping suddenly at the end of the event to a value which indicates liquefaction has occurred. PPT3 is located directly beneath the tunnel, so the low pore pressures are the result of suctions being set up as the pipe displaces vertically. PPT7 is located at the side of the tunnel, so the low pore pressures are a result of the tunnel trying to separate from the soil during horizontal shaking. Since the pore pressures rise

very quickly at the end of the test, it shows that the low values/suctions are a direct result of the tunnel trying to displace. This is backed up by the step change in tunnel displacement rate. During the test, the tunnel is seen to rise at a reasonably constant rate, but after the last cycle, the rate at which the tunnel rises falls to almost zero. Horizontal displacement is caused by the horizontal accelerations applied to the model, so after the last cycle, these will also cease.

After the earthquake, it is seen that the rate of pore pressure dissipation is greatest at PPTs 1 and 2. This is due to the pore fluid having to seep vertically upwards to reach the drainage boundary and so soil regains its strength first at depth.

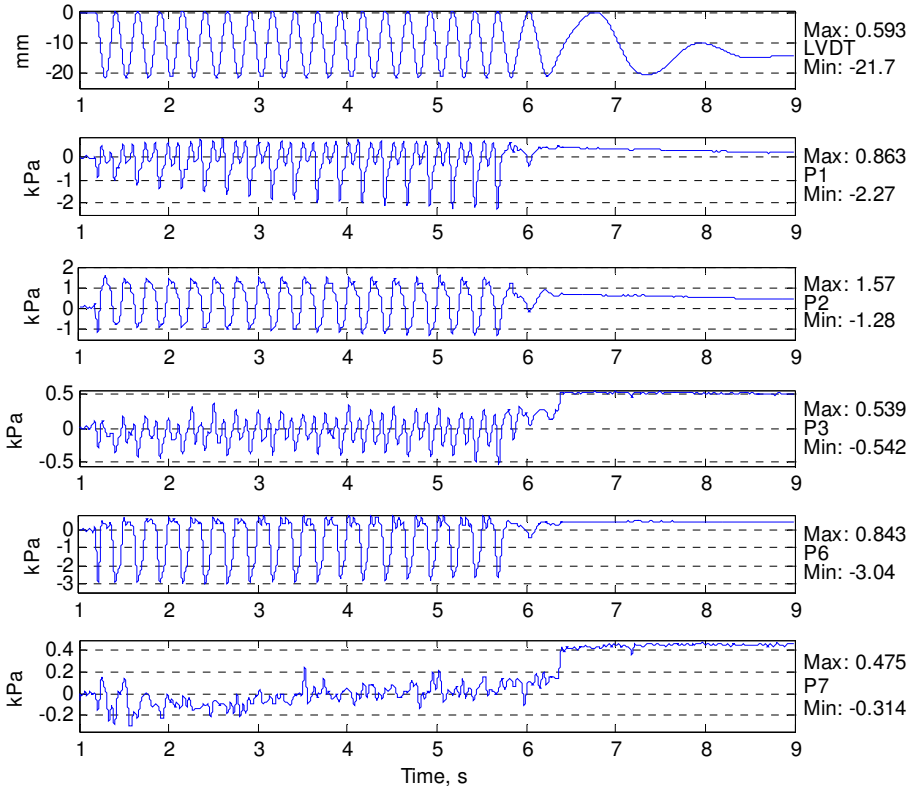

Figure 4. Excess pore pressures

Accelerations

During the test, accelerations were seen to attenuate with decreasing depth in the model. It was also observed that the phase lag increased at shallower depths and also as the earthquake progressed. The tunnel was observed to experience a greater phase lag than the surrounding soil.

Vertical Displacements.

Fig. 5 shows the vertical displacement of the tunnel during the test. It shows a linear trend during the shaking, and that almost all of the displacement occurs during the excitation. There is again quite a strong component in the fft analysis appearing at the second harmonic of the shaking frequency. After shaking has stopped, the tunnel continues to rise, but at a very low rate, which is due to flotation of the tunnel as the pore pressures dissipate.

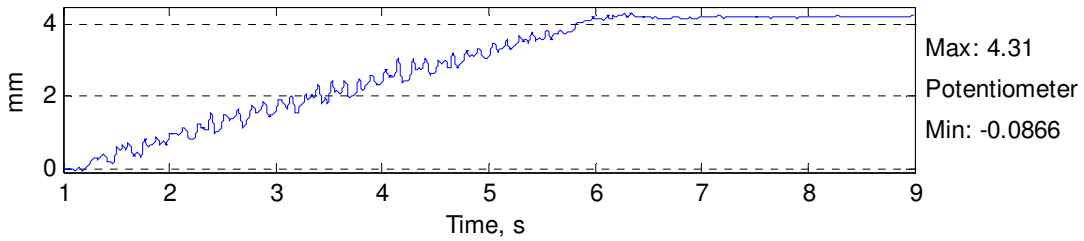

Figure 5. Vertical displacement of tunnel

Image Analysis.

The trend in vertical displacement observed by the potentiometer is confirmed by the image analysis. The position of the tunnel was tracked through the sequence and part of the sequence is presented in Fig. 6. The figure shows the vertical displacements increasing with a linear trend, but with a cyclic pattern superimposed.

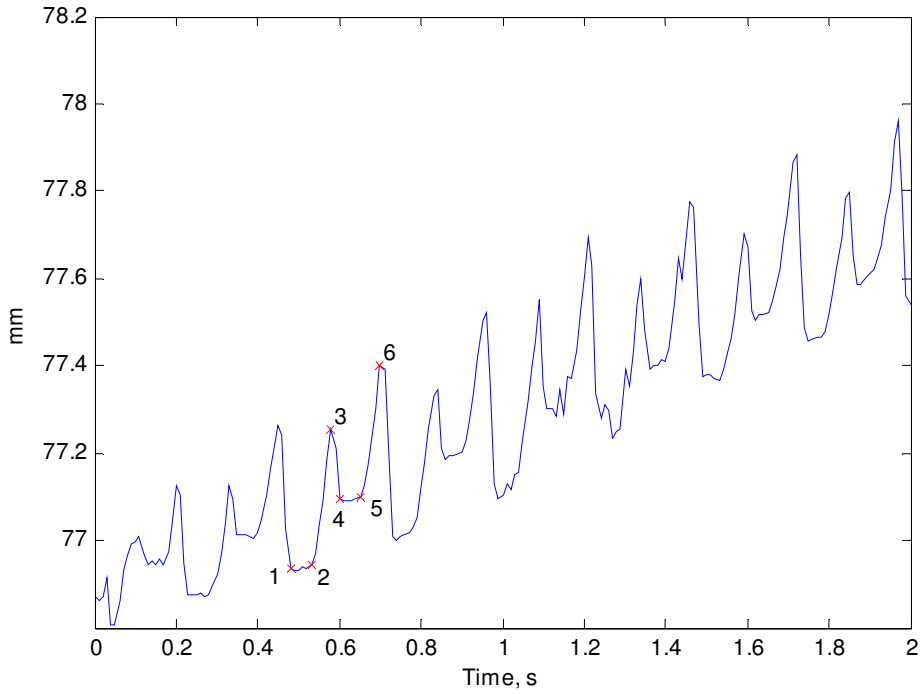

Figure 6. Vertical movement of tunnel (from geoPIV analysis)

The frequency of the periodic displacement was found to be twice the excitation frequency and shows that the vertical displacements are occurring at the same points in each half cycle.

The points 1 to 6 shown in Fig. 6 were compared to the movements of the control markers; idealising the movement of the control markers as a sine wave, the positions of points 1 to 6 are shown in Fig. 7. Since the control markers are rigidly fixed to the model container, Fig. 14 shows where points 1 to 6 occur relative to the acceleration of the container.

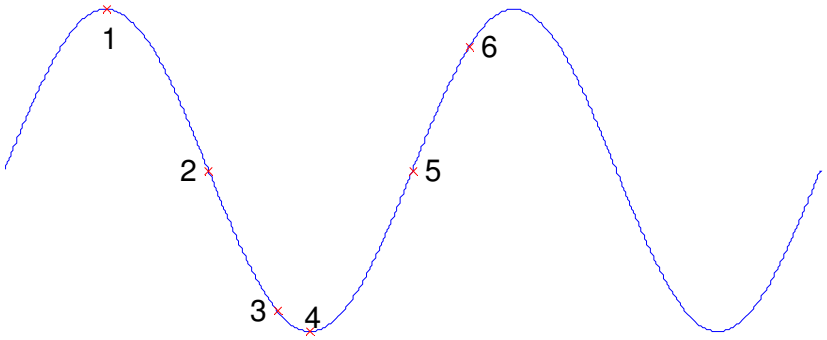

Figure 7. Position of reference points relative to input excitation

Between points 1 and 2, the tunnel is moving from its extreme right hand position to the central position. The displacements in this part of the cycle are found to be very small, with no rotation of the tunnel. There is a small amount of movement in the direction of acceleration. When examined closely, it was observed that this movement occurred close to the point of minimum acceleration.

Between points 2 and 3, the acceleration being applied reverses. The displacement field during this phase shows large lateral displacements, as the soil and tunnel move relative to the box. This may be because the soil is not rigid, so that as the container is retarded, the soil continues to move sideways. Fig. 8 shows the displacement field when this overall sideways movement has been removed. It should be noted that in this figure, the container is moving towards the left.

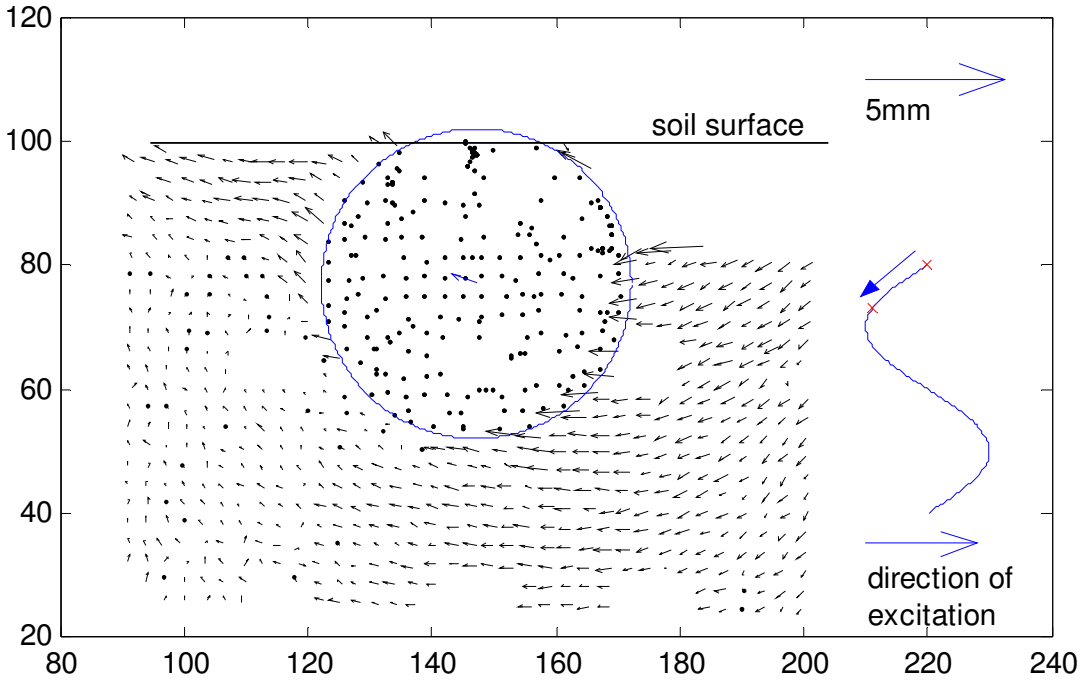

Figure 8. Displacement field between points 2 and 3

In the figure, it is observed that the tunnel moves upward and to the left. However, in front of the advancing tunnel, there is only a relatively thin band near the surface which moves. The displacements show soil close to the advancing face of the tunnel moving upward to flow into the moving band as it is 'pushed out of the way' by the tunnel. Behind the tunnel, soil appears to move into the region left by the displacing tunnel and also to flow down and around the tunnel. At this point in the cycle, the pore pressures are observed to be positive, reducing the shear capacity of the soil. The pore pressures reach values which indicate liquefaction is occurring just before the end of this phase. The tunnel therefore experiences both a buoyant force and a lateral shearing force, resulting in the observed tunnel displacement.

The displacement field between points 2 and 3 with the lateral movement of the tunnel removed showed that the displacement of the soil forced a rotation of the tunnel. Where the soil is moving in behind the tunnel, it is observed that there is no slip between the tunnel and soil. However, in front of the soil, where the soil is flowing away from the tunnel, the tunnel sides show movement relative to the soil.

From these observations it is thought that the upwards displacement in this part of the cycle is due to the soil by the side of the tunnel forcing the tunnel upwards past a region of stationary soil in front of the tunnel. The pore pressure data directly beneath the tunnel at the end of this phase shows the generation of suctions, presumably due to the tunnel uplifting.

Between points 3 and 4, the tunnel moves back downwards, in part due to the suctions generated in the previous part of the cycle. The displacements in this phase are shown in Fig. 9, with the rigid translation of soil removed.

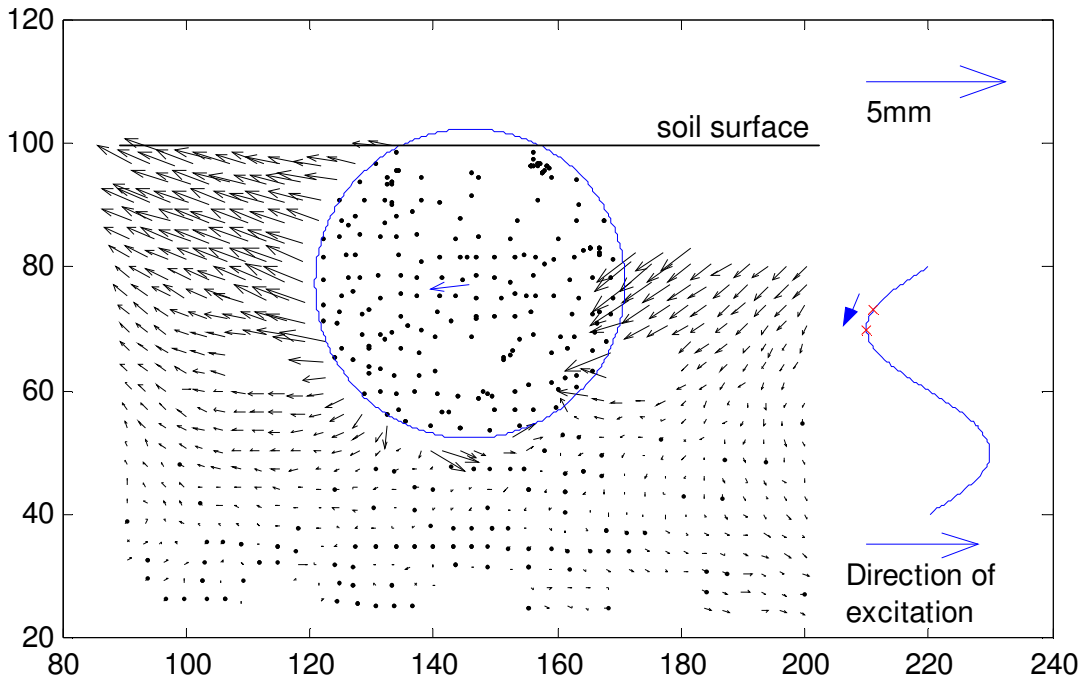

Figure 9. Displacement field between points 3 and 4

During this phase, the differential displacement which was observed in the soil layer beneath the tunnel between points 2 and 3 does not exist. This is possibly due to the suctions beneath the tunnel causing a rise in effective stress and therefore a strengthening of the soil. Since the soil is able to resist more shear, there is little or no movement. Instead, the tunnel is driven downwards by a wedge acting from behind the tunnel. The patches in this area of the plot were unsuccessfully traced, however since the mechanism is symmetrical for each half cycle of excitation, the displacement field can be assumed to be the mirror of that shown in Fig. 10, which shows the displacements between points 6 and 1 (in the next cycle). As the tunnel is driven laterally and downwards, the soil immediately in front of the tunnel is pushed out of the way, displacing almost normal to the surface of the tunnel. In front of the tunnel, the same band which was noted between points 2 and 3 remains, but has formed a shallow wedge shape, moving upwards and against the retarding acceleration.

Similar to the displacement field between points 2 and 3, when the tunnel's lateral movement is subtracted, the patches tracking the tunnel clearly show that the tunnel has rotated during this phase. The displacement field shows that although in the areas of the wedges, the tunnel is rotating such that there is very little relative movement between the soil and tunnel, directly beneath the tunnel, the tunnel moves relative to the soil.

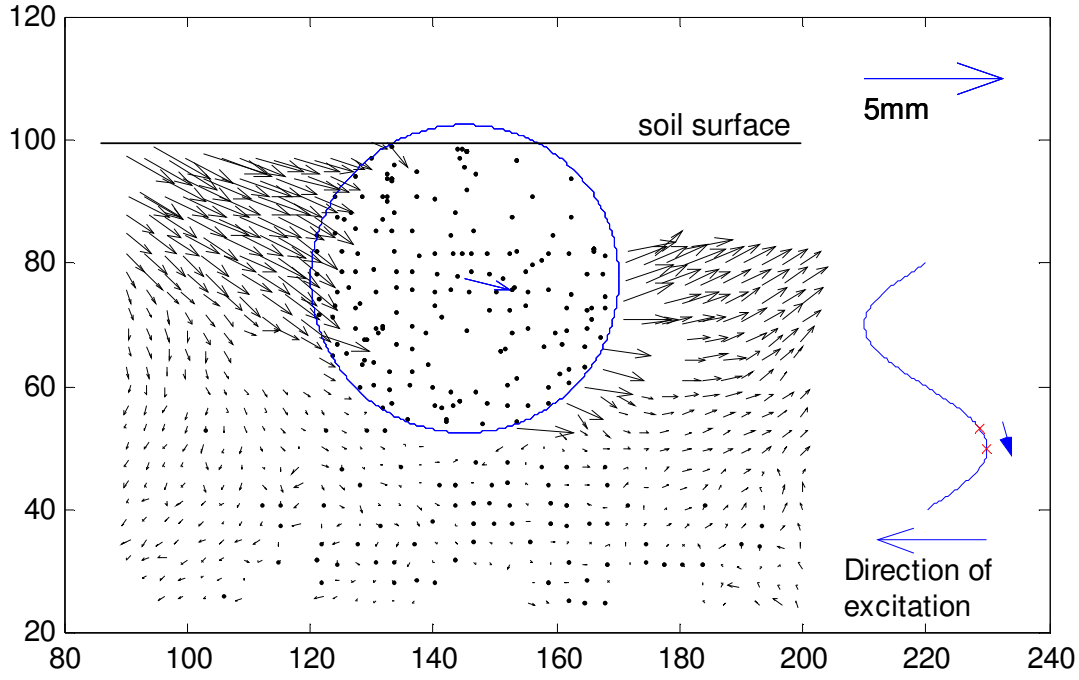

Figure 10. Displacement field between points 6 and 1

The downwards displacement in this part of the cycle is therefore caused by the suctions beneath the tunnel coupled with the downwards driving action of the wedge behind the tunnel.

It was found that the mechanisms did not change significantly throughout the earthquake. The cumulative displacement field for the uplift of the pipe during the earthquake was found and is shown in Fig. 11. It shows clearly the soil flowing round the pipe to enter the region which is left void by the pipe as it uplifts. The flow of soil round the pipe is confirmed by the movements observed of P7, as mentioned earlier. Although the overall displacement field shows the mechanism which might be

expected as a cylinder is lifted slowly out of a viscous liquid, it must be remembered that the mechanisms occurring during various phases of the cyclic excitation are very different.

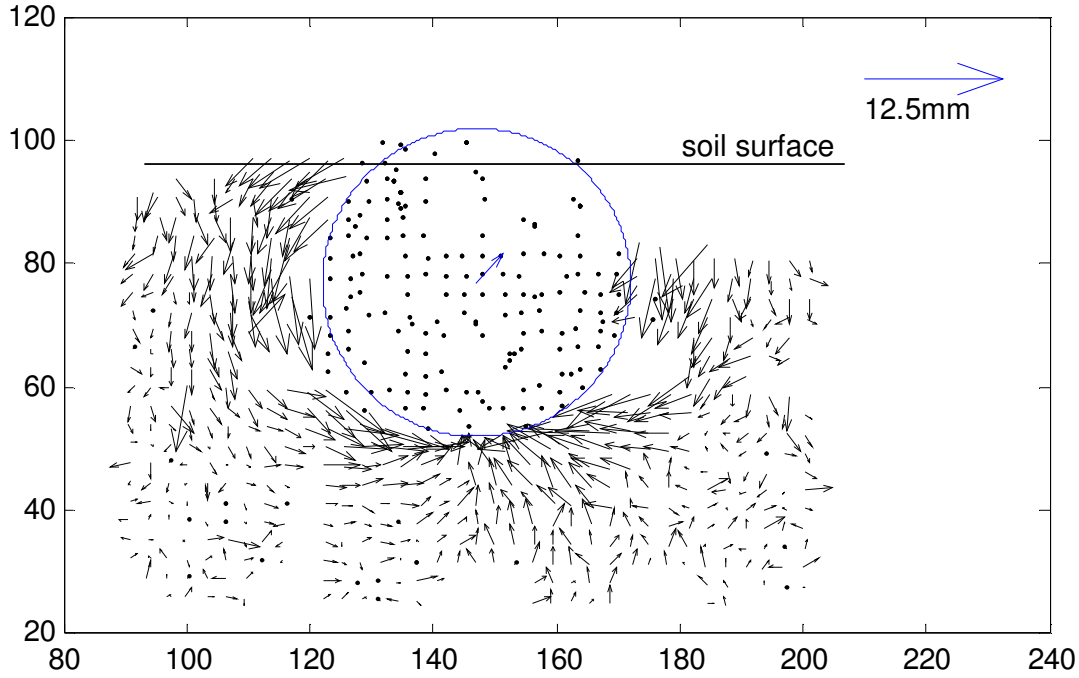

Figure 11. Cumulative displacement field at end of earthquake

CONCLUSIONS

The failure mechanism of a tunnel during a strong earthquake was investigated using a small-scale model under 1g conditions. Strong earthquakes were fired on the model, with a high speed camera acquiring a sequence of images during each of the tests. GeoPIV software was used to capture the displacement fields.

The overall displacement field showed soil flowing around the tunnel to fill the void being left by the tunnel as it moved upwards. It was found that the overall displacement field was being achieved by a three part mechanism, operating in each half cycle of excitation. Two of the phases were observed to result in tunnel movements, with upward tunnel movements occurring between points where the tunnel's acceleration has just changed direction until just before the maximum acceleration. The tunnel moves downwards from the end of the upward movement phase until maximum acceleration is reached. From maximum acceleration until the acceleration changes direction again, there is almost no tunnel movement.

ACKNOWLEDGEMENTS

The authors would like to acknowledge the help given by the staff of the Schofield Centre, in particular Dr White, for geoPIV support, and Dr Haigh for technical assistance.

REFERENCES

Arango I, Ostadam F, Cameron J, Chang CY, and Wu CL. Liquefaction of the BART Transbay tube backfill, 11th International Conference on Soil Dynamics and Earthquake Engineering, 2004

Cox C. Seismic Behaviour of Tunnels in Liquefiable Soils, Cambridge University M.Eng Project, 2002

Iai S. Simlitude for shaking table tests on soil-structure-fluid model in 1g gravitational field, Soils and Foundations, Vol. 29, No.1, pgs 105-118

Luong MP and Sidaner JF. Undrained behaviour of cohesionless soils under cyclic and transient loading, International Conference on Recent Advances in Geotechnical Earthquake Engineering and Soil Dynamics, Vol 1. phs 215-220, 1981

Seed HB and Idriss IM. Analysis of Soil Liqeufaction: Niigata Earthquake, ASCE Journal of the Soil Mechanics and Foundations Division, Vol. 93, SM3, pgs 83-108, 1967

Stewart DP, Chen YR and Jutter BL. Experience with the use of Methylcellulose as a viscous pore fluid in centrifuge models ASTM Geotechnical Testing Journal, December 1998, Vol. 21, No. 4, pgs 365-369, 1998

Teymur B and Madabhushi SPG. Soil deformation measurements around buried pipes in liquefiable soils using Particle Image Velocimetry (PIV) Proc. Int. Conf. On Problematic Soils, pgs 1003-1010, 2005

White DJ and Take WA. GeoPIV: Particle Image Velocimetry (PIV) software for use in geotechnical testing, CUED/D-SOILS/TR322, 2002

White DJ, Take WA and Bolton MD. Soil deformation measurement using particle image velocimetry (PIV) and photogrammetry, Geotechnique, Vol. 53, No. 7, pgs 619-631, 2003

Youd TL and Hoose SN. Liquefaction During 1906 San Francisco Earthquake, ASCE Journal of the Geotechnical Engineering Division, Vol. 102, GT5, pgs 425-439, 1976